AIAA JOURNAL
Vol. 47, No. 12, December 2009

Investigation of Dynamics of Lean Turbulent Premixed Flames by Rayleigh Imaging

Frank T. C. Yuen* and Ömer L. Gülder†
University of Toronto, Toronto, Ontario M3H 5T6, Canada

DOI: 10.2514/1.43255

Turbulent premixed flames of propane/air and methane/air were studied on a stabilized Bunsen-type burner to investigate the interactions between turbulence and the structure of the flame front in the thin reaction zones regime. The fuel-air equivalence ratio was varied from 0.7 to stoichiometric for propane flames, and from 0.6 to stoichiometric for methane flames. The nondimensional turbulence intensity u'/S_L covered the range from 2.7 to 24.1. The flame front data were obtained using planar Rayleigh scattering technique, and particle image velocimetry was used to measure the instantaneous velocity field of the flames. Thermal structure of the flame front was observed to change with increasing u'/S_L. The reaction zone and preheat zone thicknesses increased modestly with nondimensional turbulence intensity in both propane and methane flames. Flame front curvature statistics displayed the same Gaussian-like distribution, which centered around zero for all the flame conditions studied. Flame surface density results exhibited almost no dependence on the nondimensional turbulence intensity. It was found that the flame curvature was able to broaden the flame front and reduce the flame surface density.

I. Introduction

THE flamelet assumption has been an integral part of many numerical simulations of turbulent premixed combustion. This assumption has been used to model the complex coupling between chemistry and the heat and mass transfer. The flamelet model assumes the flame front as a thin passive surface that locally propagates with a laminar burning velocity and the combustion reactions take place within this surface. As such, the turbulent burning velocity can be approximated by the product of flamelet surface area and laminar burning velocity corrected for the effect of stretch and curvature. However, there is a growing body of experimental evidence that suggests the passive characteristics of the premixed flamelets and their laminar thermal structure may not be preserved beyond medium turbulence intensities. Also, experimental measurements of flame surface densities indicate that the flame surface area is not the dominant factor in increasing the turbulent burning velocity under the conditions corresponding to the thin reaction zones regime [1,2]. Recent experiments have shown that the flame stretch has an active role in affecting the flame front structure [3,4]. Flame stretch consists of two processes, curvature and strain, which have dominant roles in the dynamics of the turbulent premixed flames [5]. Dinkelacker et al. [6] have shown that medium- and large-scale turbulent eddy-generated strain effects have much more influence than diffusive effects from small scale-eddies. Soika et al. [4], on the other hand, have suggested that the flame reacts more to flame curvature than to the effects of small-scale turbulent eddies. A recent review by Driscoll [7] has summarized the concept of flamelet wrinkling by flame-vortex interactions. This interaction controls the stretch rate and the eddy residence time during which the stretch rate is applied. The review further stated that thermodiffusive effects are observed to be important in highly turbulent flames, which means turbulent eddies and the flame stretch are both affecting turbulent premixed flames. However, there is no consensus on whether these effects are competing events, acting alone or in combination.

The objectives of this study are to evaluate flame front temperature profiles and their temperature gradients, thermal flame front thickness, flame curvature statistics, and flame surface density. These evaluations will provide means to understand the interaction between turbulence field characteristics and flame front dynamics as well as the effect of turbulence and curvature on the flame front structure. Thus, the validity range of the flamelet model for various flame conditions could be assessed.

II. Experimental Method

Premixed turbulent conical flames were produced by an axisymmetric Bunsen-type burner with an inner nozzle diameter of 11.2 mm. The main flame was anchored to the burner nozzle by an annular pilot flame under different turbulent conditions. A premixed propane/air or methane/air pilot flame was used for low-turbulent intensities, and a premixed ethylene/air pilot flame was used for high-turbulent intensities. The premixed propane/air flame was studied at equivalence ratios from 0.7 to 1.0, and methane/air flame from 0.6 to 1.0. Turbulence level was regulated by perforated plates that were located at 3-diameter lengths upstream of the burner nozzle. These provided the experimental conditions of the nondimensional turbulence rms velocity (u'/S_L) ranged from 2.7 to 24.1, which correspond to conditions of the corrugated flamelets and thin reaction zones regimes as described by Peters [8].

A. Particle Image Velocimetry Setup

Particle image velocimetry (PIV) was used to measured instantaneous velocity field of the flames for all experimental conditions studied. These conditions are summarized in Table 1. The PIV experiment was conducted separately from the Rayleigh scattering experiments due to the presence of seeding particles. The system consisted of a double-pulsed second harmonic (532 nm) Nd:YAG laser (New Wave Research Solo) working at an energy level of 50 mJ/pulse and a frequency of 15 Hz, which gives a pulse duration of 0.01 μs and two laser pulses separation of 10 μs; a charge-coupled device (CCD) camera (Flow Sense M2 8-bit) with an array size of 1600×1186 pixels and equipped with a camera objective (Nikkor, $f = 60$ mm, $f_{\#} = 2.8$). This optical setup was used to capture the flow condition above the nozzle exit with a view area of 15.7 mm $\times$ 11.6 mm and a resolution of 9.8 μm/pixel. Submicrometer olive oil droplets were generated by a nebulizer as seeding particles. An interrogation region of 32×32 pixels was used

Presented as Paper 243 at the 47th AIAA Aerospace Sciences Meeting including The New Horizons Forum and Aerospace Exposition, Orlando, FL, 5–8 January 2009; received 15 January 2009; revision received 27 July 2009; accepted for publication 4 August 2009.

*Ph.D. Candidate, Institute for Aerospace Studies, 4925 Dufferin Street.
†Professor, Institute for Aerospace Studies, 4925 Dufferin Street. Senior Member AIAA.

Table 1 Summary of experimental flow and flame conditions

Flame [a]	ϕ [b]	Λ, mm [c]	λ, mm [d]	η, mm [e]	δ_L^o, mm [f]	u'/S_L	Ka [g]	Re_Λ [h]
M1	1.0	1.62	0.45	0.05	0.45	3.2	1.1	98
M2	0.9	1.62	0.45	0.05	0.48	3.7	1.4	97
M3	0.8	1.62	0.45	0.05	0.54	4.7	2.2	97
M4	0.7	1.62	0.45	0.05	0.68	6.4	4.2	97
M5	0.6	1.62	0.45	0.05	1.00	10.8	11.9	96
M6	1.0	1.64	0.44	0.05	0.45	3.3	1.1	101
M7	0.9	1.64	0.44	0.05	0.48	3.7	1.4	100
M8	0.8	1.64	0.44	0.05	0.54	4.7	2.2	100
M9	0.7	1.64	0.44	0.05	0.68	6.6	4.3	100
M10	0.6	1.64	0.44	0.05	1.00	11.0	12.1	99
M11	1.0	1.79	0.46	0.03	0.45	7.3	3.4	242
M12	0.9	1.79	0.46	0.03	0.48	8.2	4.3	241
M13	0.8	1.79	0.46	0.03	0.54	10.4	7.0	240
M14	0.7	1.79	0.46	0.03	0.68	14.4	13.4	239
M15	0.6	1.79	0.46	0.03	1.00	24.1	37.7	238
P1	1.0	1.61	0.42	0.06	0.34	2.7	0.8	84
P2	0.9	1.61	0.42	0.06	0.36	3.0	1.0	84
P3	0.8	1.61	0.42	0.06	0.40	3.7	1.5	83
P4	0.7	1.61	0.42	0.06	0.48	5.1	2.9	83
P5	1.0	1.53	0.41	0.05	0.34	3.4	1.2	102
P6	0.9	1.53	0.41	0.05	0.36	3.9	1.5	101
P7	0.8	1.53	0.41	0.05	0.40	4.7	2.2	101
P8	0.7	1.53	0.41	0.05	0.48	6.6	4.3	100
P9	1.0	1.75	0.44	0.03	0.34	6.7	3.0	229
P10	0.9	1.75	0.44	0.03	0.36	7.6	3.8	227
P11	0.8	1.75	0.44	0.03	0.40	9.3	5.7	226
P12	0.7	1.75	0.44	0.03	0.48	12.9	11.0	225
P13	0.7	1.83	0.46	0.03	0.48	12.5	10.3	229
P14	0.7	1.37	0.41	0.02	0.48	16.2	17.7	222
P15	0.7	1.77	0.43	0.02	0.48	17.5	17.4	309
P16	0.7	1.54	0.44	0.02	0.48	20.3	23.3	311

[a]Flame M refers to methane/air flames, whereas P refers to propane/air flames.
[b]ϕ is the fuel-air equivalence ratio.
[c]Λ is the integral length scale.
[d]λ is the Taylor length scale.
[e]η is the Kolmogorov length scale.
[f]δ_L^o is the unstretched laminar flame thickness.
[g]Ka is the Karlovitz number.
[h]Re_Λ is the Reynolds number based on u' and Λ.

together along with the image scale factor of 1.326 and the CCD pixel pitch of 5.56 μm. The multiplication of these terms yields the actual PIV resolution of about 0.24 mm, which is the smallest velocity structure that can be resolved. The turbulence length scales were estimated using the velocity field data from the PIV measurements, which provided u'. Two-point correlation functions of u' were calculated along the length of the image. Then, these functions were integrated to where they first crossed zero so that the integral length scales Λ were estimated. The Taylor length scales (λ) were evaluated by constructing an osculating parabola for the two-point correlation functions. The distance to which the parabola crosses zero is the Taylor length scale. The mean flow velocity at the nozzle exit was varied between 14.5 m/s and 17.9 m/s.

B. Rayleigh Scattering Setup

Planar laser Rayleigh scattering was used to capture flame front images as shown in Fig. 1 [9,10]. This setup consisted of a third

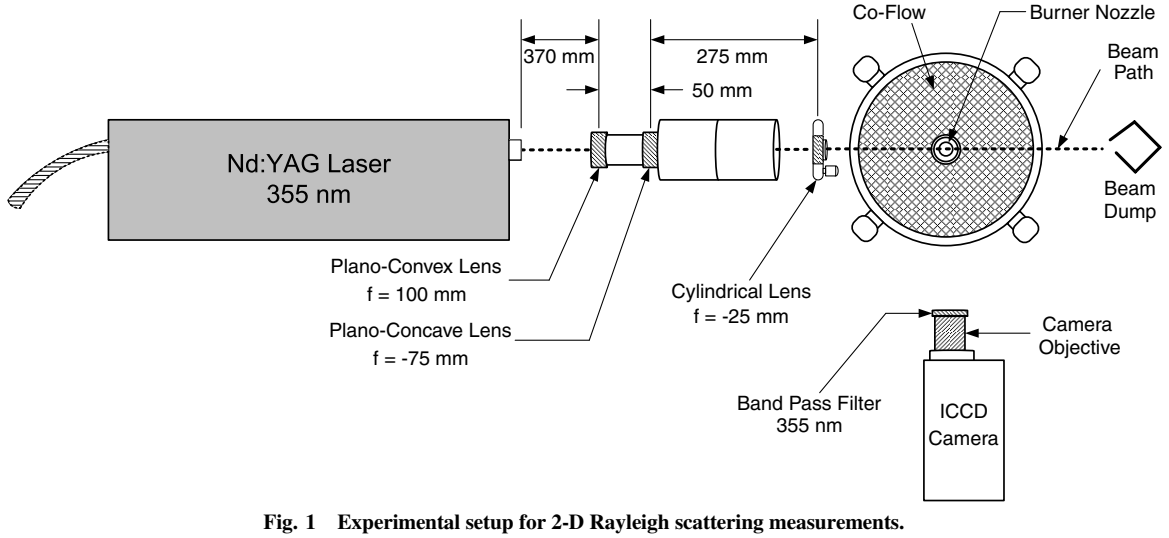

Fig. 1 Experimental setup for 2-D Rayleigh scattering measurements.

harmonic (355 nm) Nd:YAG laser (Spectra-Physics Quanta-Ray Lab-170) working at an energy level of 305 mJ/pulse and a frequency of 10 Hz; a laser sheet of 60 mm high and 150 μm thick was produced by a set of beam-shaping optics (plano-concave lens $f = -75$ mm, plano-convex lens $f = 100$ mm, plano-concave cylindrical intensified CCD (ICCD) lens $f = -25$ mm). An ICCD camera (Lavision NanoStar) with an array size of 1280×1024 pixels positioned at 90 deg to the scattered light, and equipped with a UV camera objective (Sodern Cerco 2085, $f = 94$ mm, $f_{\#} = 4.1$). A capture area of 57 mm $\times$ 46 mm and a resolution of 45 μm/pixel were achieved, which is the maximum resolution of the Rayleigh imaging system. This was found using the contrast transfer function (CTF) that corresponds to 22 line-pairs/mm at CTF of 10%. Hence, the limiting resolution for the Rayleigh scattering measurements would be the laser sheet thickness that is 150 μm. Because of this optical setup, the flame was imaged at three different sections along the centerline of the nozzle. Each of these sections has an area of 44 mm $\times$ 22 mm. The centers of the three sections are 66.5, 96.5, and 121.5 mm above the burner nozzle. These flame sections were labeled as low, middle, and top, respectively. Three hundred images were captured for each of the flame sections for all the experimental conditions. The signal-to-noise ratio for the reactants is about 23.8 and 14.3 for the products. This is found by calculating the ratio between the mean and standard deviation for an area of 2500 pixels in the product and reactant regions of the flame. Typical Rayleigh scattering intensity is about 260 counts for reactant pixels and 72 counts for product pixels.

Raw Rayleigh scattering images were first processed using a nonlinear sliding average filter for noise reduction. The 3×3 filter size was chosen because similar results were obtained compared with filter sizes of 2×2 and 4×4. Rayleigh scattering signal is linearly proportional to the total number density of the molecules weighted for their Rayleigh scattering cross sections. With the assumption of negligible pressure changes across the flame front, the ideal gas law was used to find the temperature of the flame [9,11,12] using Eq. (1) [4]

$$T_{\text{flame}} = \underbrace{\frac{\left(\sum_i \sigma_i \chi_i\right)_{\text{mix}}}{\left(\sum_i \sigma_i \chi_i\right)_{\text{air}}}}_{k} \cdot T_{\text{air}} \underbrace{\frac{(I_{\text{air}} - I_{\text{back}})}{(I_{\text{flame}} - I_{\text{back}})}}_{I} \tag{1}$$

where T_{flame} is the temperature evaluated for each pixel in each flame image, σ_i is the Rayleigh scattering cross section for each molecule i, χ_i is the mole fraction of different species, I_{flame} and I_{air} are the Rayleigh scattering signal intensity of the flame and a calibration image with air at temperature T_{air}, respectively. I_{back} is the background signal intensity, which consisted of the dark noise of the ICCD camera, the laboratory background light, and laser reflections. Because of its parasitic nature in the experimental setup, I_{back} was estimated by setting $T_{\text{flame}} = T_{\text{ad}}$ (adiabatic flame temperature) and solving Eq. (1) in the product region of the each flame image. This technique of calculating I_{back} have been reported by Knaus et al. [13]. The background signal was approximately 26 counts and the variation was less than ± 3 counts throughout the flame image, so it is reasonable to use a single background count for the entire image.

The Rayleigh scattering cross sections that had been tabulated by Sutton and Driscoll [14] were used. The variation of the different combustion species across the flame front was obtained through a 1-D laminar flame simulation with the Cantera package that uses the GRI-3.0 mechanism [15]. From these data, the variation of the effective Rayleigh scattering cross sections [k in Eq. (1)] with temperature were calculated for methane and propane flames as shown in Figs. 2 and 3. The peaks of the intensity probability density function of the intensity ratio [I in Eq. (1)] that correspond to the burned and unburned gases were determined. These peak intensity ratio values were then related to the burned and unburned gas temperatures. In this way, relationships of k versus I were established for different equivalence ratios and fuels. So for each I value, there was a corresponding k value for calculating T_{flame} at each pixel. A processed instantaneous Rayleigh scattering temperature image is shown in Fig. 4.

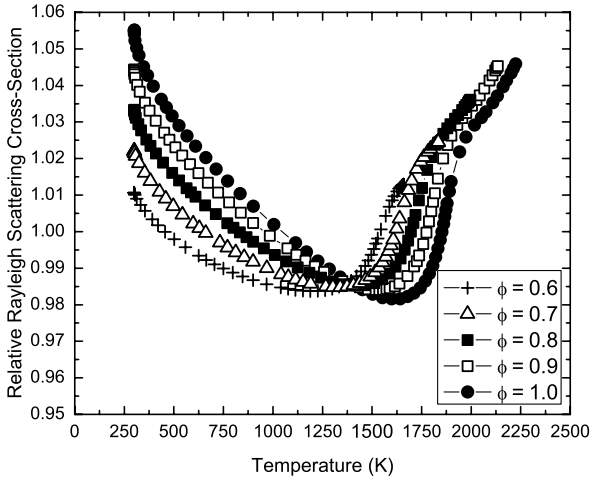

Fig. 2 Variation of k with temperature for methane flames.

III. Data Analysis

A. Two-Dimensional Flame Front Thickness and Gradient

The Rayleigh scattering images were processed to provide instantaneous temperature gradients ∇T at $c = 0.5$ and 0.3, and progress variable gradients ∇c at $c = 0.1$–0.9, where $c = (T - T_u)/(T_b - T_u)$. T is the instantaneous temperature, T_b is the burned gas temperature, and T_u is the unburned gas temperature. Thermal flame front thicknesses $\delta_{\text{th},c}$ at a certain progress variable c were calculated using Eq. (2)

$$\delta_{\text{th},c} = \frac{T_b - T_u}{|\nabla T|_c} \tag{2}$$

where $|\nabla T|_c$ is the temperature gradient at a given progress variable. Galley [16] has shown that the maximum temperature gradients are nearly equal to the ones found on the progress variable contour of $c = 0.5$. Kim and Pitsch [17] have defined the reaction zone on the $c = 0.5$ contour by defining the flame normal on the contour for their direct numerical simulation study of turbulent premixed flames. Dinkelacker et al. [6] have characterized the reaction zone thickness at $c = 0.5$ and suggested the sampling of temperature gradients along a single c contour to prevent an overrepresentation of flame regions with low gradients when sampling in a range of c values. The same authors have also chosen $c = 0.25$ the location of preheat zone, whereas Soika et al. [4] have used $c = 0.3$. Galley [16] has shown that both $c = 0.25$ and $c = 0.3$ temperature gradients share the same trend, although their values are different. Thus, the flame front

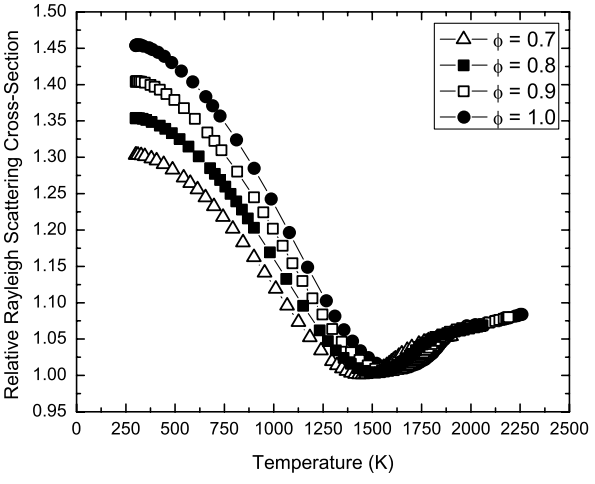

Fig. 3 Variation of k with temperature for propane flames.

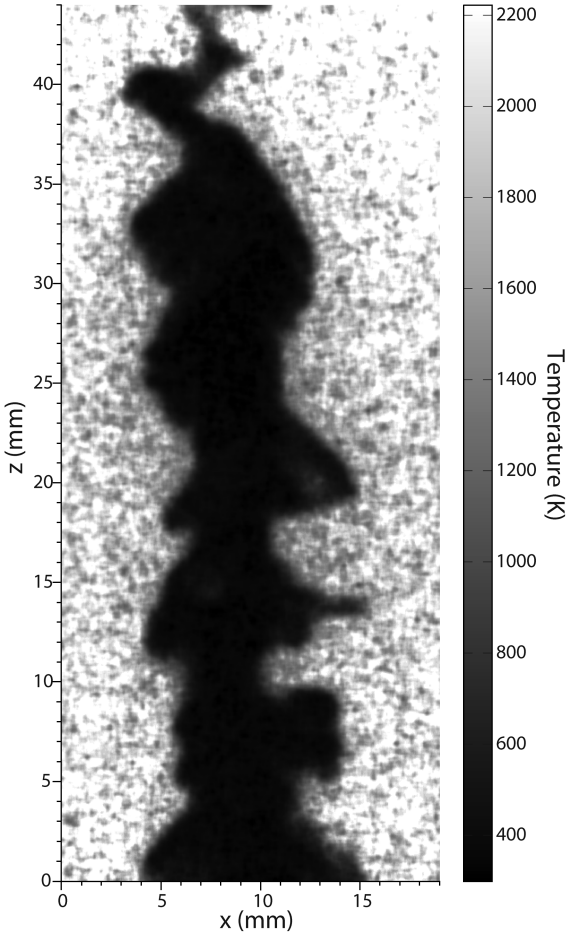

Fig. 4 Instantaneous processed Rayleigh scattering temperature image for flame condition M1.

thickness at $c = 0.5$ is considered as the reaction zone thickness, whereas the one at $c = 0.3$ is regarded as the preheat zone thickness in this study.

The c contours were found using an edge detection algorithm. Two-dimensional ∇T and ∇c were extracted at each point along the c contours. T_u and T_b were found from the distinct peaks in temperature probability density function (PDF) of each image, which corresponds to the most probable temperature values in the unburned and burned gases. Laminar thermal flame thicknesses δ_L^o were calculated from the temperature profiles across a 1-D laminar flame simulation, which was performed using the Cantera package. The error introduced by the Rayleigh imaging system was estimated using the analysis method described by Wang and Clemens [18], in which dissipative structures larger than the laser sheet thickness of 150 μm were found to have a relative error of 9% in flame front thickness and 8% relative error for temperature gradients. The overall error, including the random error and propagation of error, was found to be 19–23% for flame front thickness and 11–13% for temperature gradient measurements with a 95% confidence interval.

B. Two-Dimensional Flame Front Curvature

Local flame front curvature κ at each pixel point along the $c = 0.5$ contour was calculated. The $c = 0.5$ contours that were used for curvature evaluation were filtered by a zero-phase digital filter, which processed the contours in both forward and reverse directions. These provided no phase distortion and doubled the filter order. The filter length was chosen to be five points, which provided a filter order of eight. The derivative curves were filtered again using the same filter and then curvatures were evaluated using Eq. (3)

$$\kappa = \frac{\dot{x}\,\ddot{y} - \dot{y}\,\ddot{x}}{(\dot{x}^2 + \dot{y}^2)^{3/2}} \tag{3}$$

where $\dot{x} = \mathrm{d}x/\mathrm{d}s$ and $\ddot{x} = \mathrm{d}^2x/\mathrm{d}s^2$ are the first and second derivatives with respect to s, which is the flame contour length measured from a fixed origin on the flame front [19,20]. The uncertainty in finding curvature is mainly due to the laser sheet thickness of 150 μm, which is the minimum radius of curvature that can be resolved. This corresponds to the limiting curvature of $6.6\dot{7}$ mm^{-1}, and the mean standard deviation of the curvature statistics is about 1.74 mm^{-1}. The uncertainty in estimating curvature below the limiting curvature is about 3% with a 95% confidence interval.

C. Two-Dimensional Flame Surface Density

Flame surface density (FSD) is a measure of the flame surface area per unit volume. This quantity describes the wrinkling of the flame front surface by turbulence [21–23]. Thus, the increase in local burning rate as a result of the wrinkling of the flame front surface is described by the following:

$$\langle\dot{\omega}\rangle(x) = \rho_r S_L^o I_o \Sigma(x) \tag{4}$$

where $\langle\dot{\omega}\rangle$ is the mean rate of conversion of reactants into products per unit volume (or the local burning rate), ρ_r is the density of reactants, S_L^o is the unstretched laminar burning velocity, I_o is the factor dependent on distribution of flame curvature and strain rates over the flamelet surface (stretch factor), and $\Sigma(x)$ is the FSD in the axial direction [21,22,24].

For the current experiments, two different FSD methods were employed. They are the flame length and flame zone area method by Shepherd [25] and the gradient of progress variable ∇c method [26].

The method by Shepherd is a 2-D estimate of FSD that is a direct measure of the flame front length and the flame zone area as functions of the mean progress variable $\bar{c}$. Although the true definition of FSD is the flame surface area to volume ratio, the 2-D estimate is still considered as a reasonable approach. The flame zone area $A(\bar{c})$ was determined from maps of $\bar{c}$ that were obtained by averaging 300 c images of the flame. As such, $A(\bar{c})$ values were calculated from the histogram of $\bar{c}$ values and the known area of each pixel (0.002025 mm^2). As for flame front length $L(\bar{c})$, each flame front edge was divided into equal segments of 1 pixel length (0.045 mm). Then, the flame front edge was superimposed onto to the $\bar{c}$ map, and each flame front segment was assigned with a $\bar{c}$ value. From this, $L(\bar{c})$ was found in the similar manner to $A(\bar{c})$. So the 2-D estimate of FSD was found using the following:

$$\Sigma(\bar{c}) = \frac{L(\bar{c})}{A(\bar{c})}\frac{1}{n_f} \tag{5}$$

where n_f is the number of flame images analyzed [23,25,27].

The gradient of c method measures the spatial variation of FSD across the flame front [26]. This FSD was found using the following:

$$\Sigma = \langle\Sigma'\rangle = \langle|\nabla c| \cdot \delta(c - c_f)\rangle \tag{6}$$

where Σ' is the instantaneous local FSD, ∇c is the gradient of progress variable that is the spatial flame front gradient, and $\delta(c - c_f)$ is the instantaneous flame front location where δ is the Kronecker delta [26,28,29]. Because Eq. (6) is generalized for a 3-D surface, the instantaneous 2-D FSD Σ'_{xy} needs to be corrected by the individual flame front orientation angle θ. This angle was found by calculating the ∇c in both x and y directions, so that the unit normal vectors for both directions were found by $N_i = \nabla c_i/|\nabla c|$. From these unit normal vectors, θ_{xy} can be calculated and Σ' was found using [22,28,29]

$$\Sigma = \langle\Sigma'\rangle = \left\langle\frac{\Sigma'_{xy}}{\cos\theta_{xy}}\right\rangle \tag{7}$$

From these two FSD methods, the total burning rate can be estimated by integrating $\Sigma(\bar{c})$ across the flame front. The overall error for the gradient of c method was about 15–21% with a 95% confidence interval.

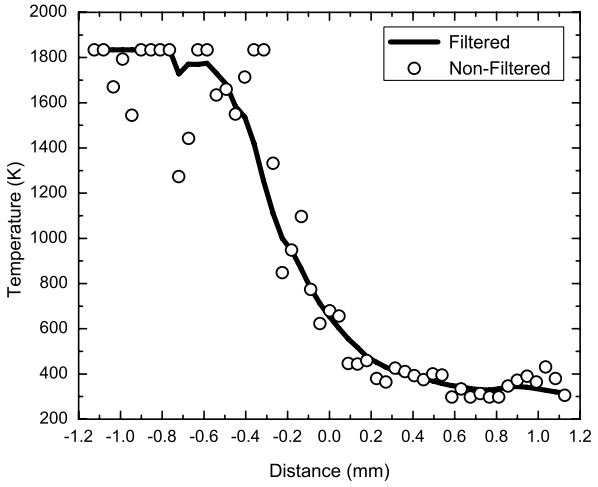

Fig. 5 Instantaneous temperature profile for flame condition M9. Circles are the raw data and the line represents 3 × 3 nonlinear sliding average filtered data.

IV. Results and Discussion

A. Average Temperature Profiles

After the Rayleigh scattering images were processed, instantaneous temperature profiles (Fig. 5) were extracted from 300 methane flame images for each nondimensional turbulence intensity u'/S_L at 3.2, 6.6, and 24.1. These profiles were then averaged and normalized by their respective adiabatic flame temperatures to provide the curves in Fig. 6. It is interesting to note that there is an increase in the averaged temperature in the preheat zone of the temperature profile for $u'/S_L = 24.1$. The similar phenomenon is also observed by Kortschik et al. [30], in which the averaged temperature profiles for methane/air flame for u'/S_L at 3.5, 9.2, and 18.7 are found to have about 20 K difference between the largest and lowest u'/S_L temperature profiles. This observation confirms the previous results that implied that there are transport phenomena such as small turbulent eddies that enter the preheat zone and enhance the transport of the heat from the reaction zone by transporting preheated gases ahead of the reaction zone over a distance the same size as their own [8,30,31].

B. Flame Front Thickness

Flame front thicknesses estimated from 2-D temperature gradients using planar Rayleigh scattering measurements were gathered to provide PDFs (see Fig. 7), in which peak (most probable) values were

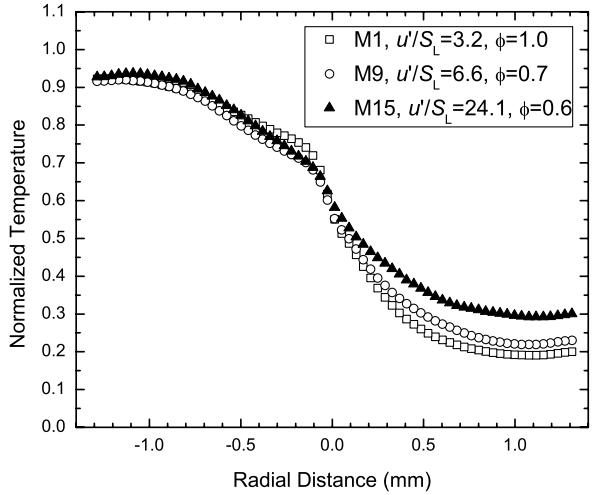

Fig. 6 Averaged temperature profiles across the methane/air flame front at different u'/S_L. Center of the temperature profile was chosen where the maximum temperature gradient was located.

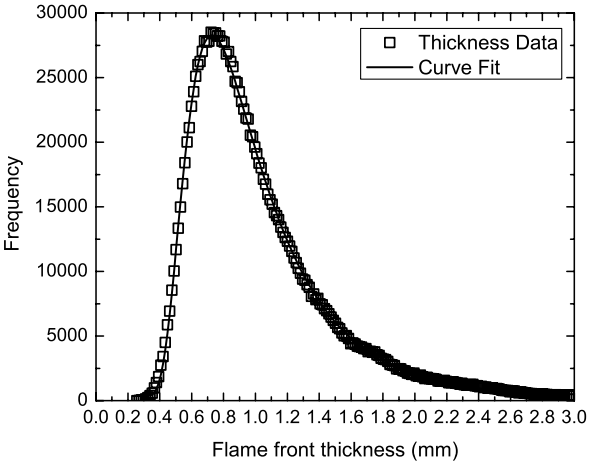

Fig. 7 Reaction zone thickness PDF with curve fit for flame condition M4, $\phi = 0.7$ and $u'/S_L = 6.4$.

extracted and appear to have a small dependence on u'/S_L. The variation of the reaction zone thickness for methane flames is shown in Fig. 8. For all three sections of the flame, the reaction zone thickness seems to be increasing slightly with u'/S_L. The similar trend was also observed for reaction zone thickness of propane flames. As for the preheat zone thickness for propane flames, the same mild dependence on nondimensional turbulence intensity was observed in Fig. 9. The preheat zone thickness for methane flames was noticed to have the same trend as well. These figures show that the thickening process with increasing turbulence is comparable for both the reaction zone and the preheat zone, although a recent numerical simulation study reports that the thickening process in the reaction zone is much weaker than in the preheat zone [17]. It is suggested by de Goey et al. [31] that 2-D thickness measurements were systematically higher than those of the 3-D measurements by about 10–20% on methane/air flames for u'/S_L about 5–19. This implies that 2-D measurements are prone to out-of-plane movements of the flame. However, the same study also showed that 2-D and 3-D flame thickness measurements have very similar behavior with u'/S_L. Although the 2-D flame front thickness measurements reported may not be able to fully capture the 3-D flame front structure, these data should be able to provide useful information describing the actual flame front structure changes induced by turbulence.

C. Temperature Gradients

The temperature gradients for the reaction zone and the preheat zone show a decreasing trend as the nondimensional turbulence

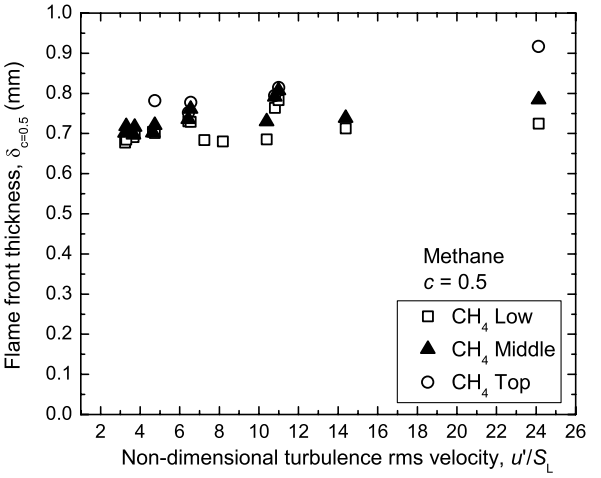

Fig. 8 Peak reaction zone thicknesses for methane flames as a function of u'/S_L at different sections.

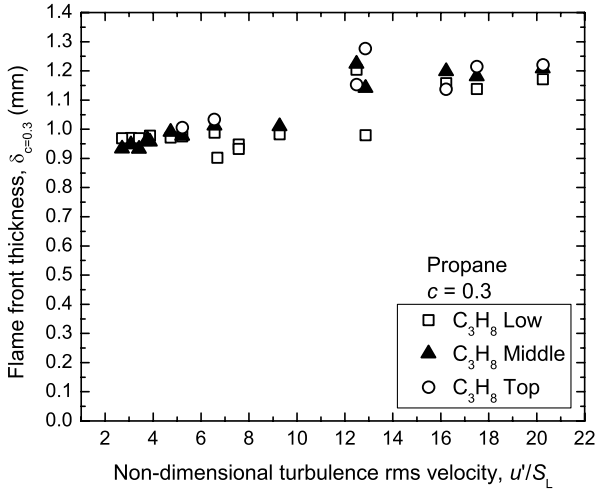

Fig. 9 Peak preheat zone thickness for propane flames as a function of u'/S_L at different sections.

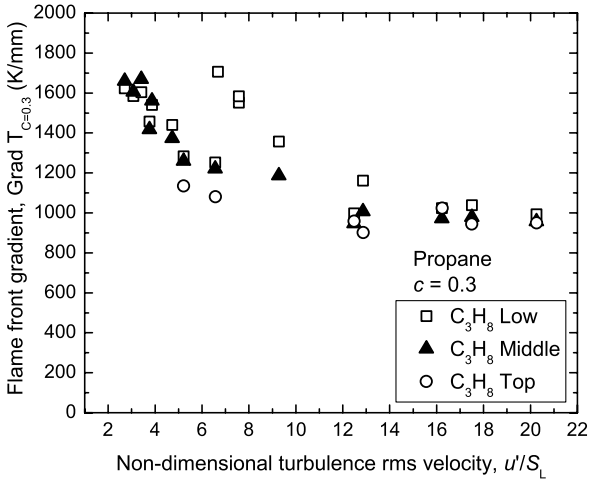

Fig. 11 Mean preheat zone temperature gradients for propane flames as a function of u'/S_L at different sections.

intensity u'/S_L increases. The dependence of temperature gradients on u'/S_L are much more pronounced than those of the flame front thicknesses. The change in reaction zone temperature gradient for methane flames is shown in Fig. 10. The temperature gradients are decreasing with u'/S_L and seem to be leveling off at high u'/S_L conditions for all three sections of the flame. The same trend is observed for the preheat zone temperature gradients of propane flames as shown in Fig. 11. The decrease in temperature gradient means that the thermal flame front structure is being thickened. The comparison between the reaction zone and preheat zone gradient figures shows that the rate of thickening is very similar for the two different layers of both fuels. However, because Lewis number is less than unity for lean methane flame and larger than unity for lean propane flame [32], factors such as curvature and strain also play a role in affecting the flame front structure. Flame stretch is suggested to be the influential factor for changes in the flame front structure when the turbulent eddies are not able to affect the reaction zone [4,5]. Therefore, there is a need to identify the effects of the turbulent eddies, curvature, and strain on the gradient and thickness separately.

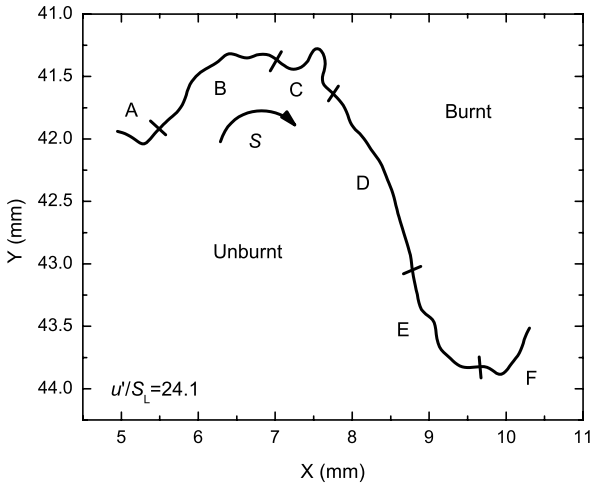

Fig. 12 Curvature contour for flame condition M15.

D. Flame Front Curvature

An example of the flame curvature contour evaluated at $c = 0.5$ is shown in Fig. 12. Different sections of this contour were labeled for flame condition M15, and the instantaneous curvature values along these contours are shown in Fig. 13. Local curvature values were observed to be equally distributed among positive and negative curvature values. The PDFs of propane and methane flame surface curvatures for all three sections are similar to Fig. 14. These curvature PDFs display Gaussian-like distributions at all turbulent intensities that are similar to those reported elsewhere [19,27]. Because of the Gaussian nature of the PDFs, the ensemble average was used for each data set and the mean flame curvature for propane flames is shown in Fig. 15. The mean propane flame curvature were observed to be

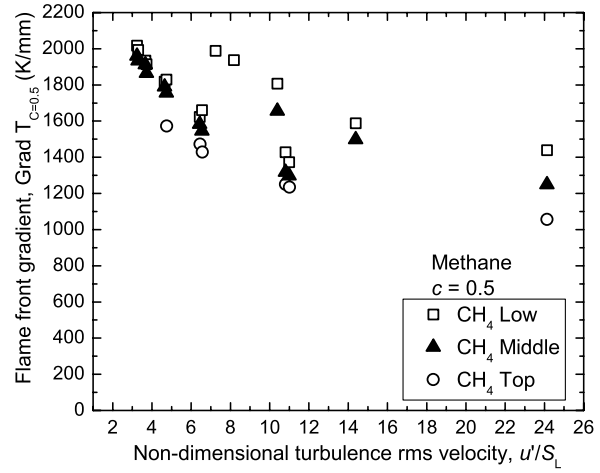

Fig. 10 Mean reaction zone temperature gradients for methane flames as a function of u'/S_L at different sections.

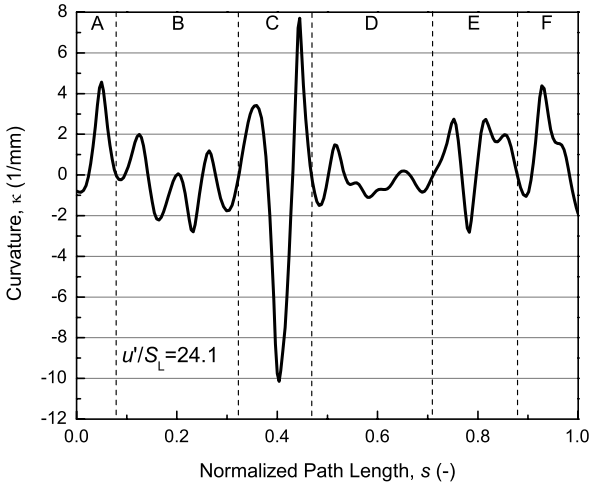

Fig. 13 Instantaneous curvature values along the curvature contour for flame condition M15 as a function of normalized path length s.

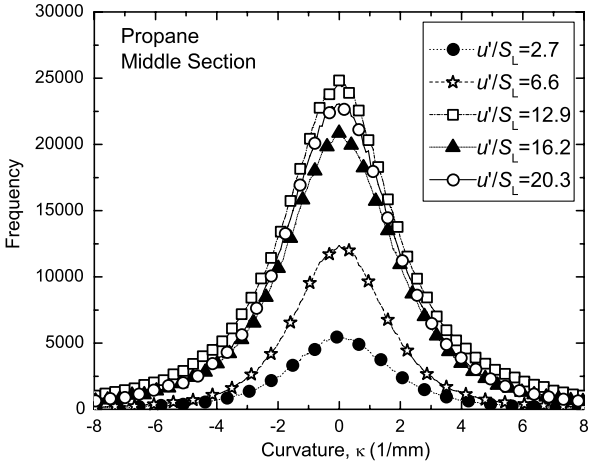

Fig. 14 PDFs of curvature for propane flames at different u'/S_L at the middle section.

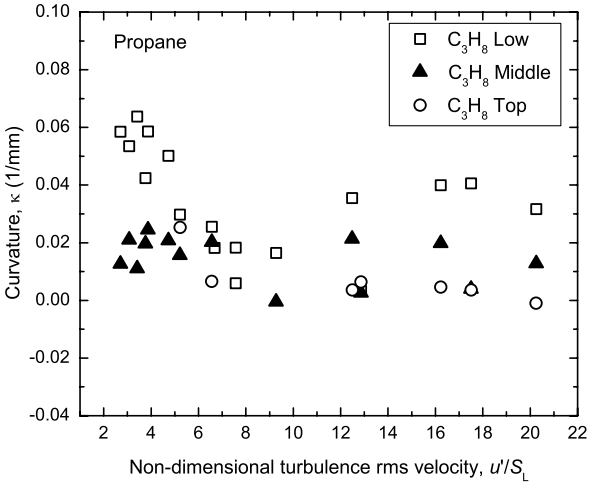

Fig. 15 Mean flame curvature as a function of u'/S_L for propane flames at different sections.

decreasing with nondimensional turbulence intensity and approached zero. The similar trend was also observed for the mean methane flame curvature results (Fig. 16) at different sections of the flame. However, the methane flame curvatures showed a steeper decrease with increasing u'/S_L. It can be argued that the measured curvature statistics are 2-D quantities that may not be able to describe a 3-D phenomenon. However, Chen et al. [33] report that 2-D and 3-D curvature PDFs are very similar.

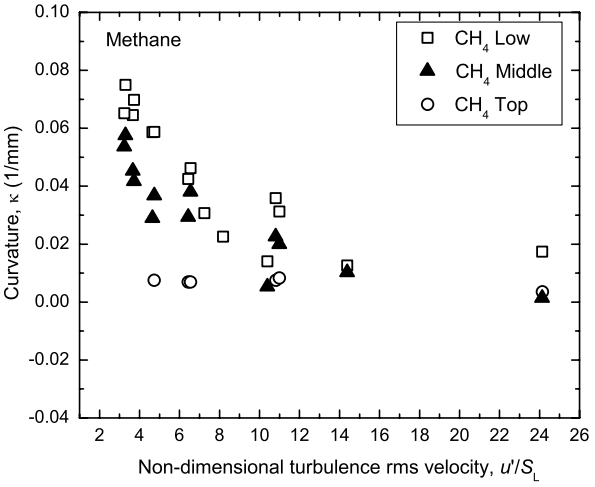

Fig. 16 Mean flame curvature as a function of u'/S_L for methane flames at different sections.

E. Flame Surface Density

The FSD data for methane flames obtained using the two methods as a function of c are shown in Figs. 17 and 18. Both methods were observed to have similar trends, in which FSD decreases as nondimensional turbulence intensity increases. The same tendency was also noticed for propane flames. The peak values of FSD for both fuels, evaluated by Shepherd's method [25] or by the gradient of the progress variable [26], did not change much with u'/S_L (see Fig. 19). The similar trend can be seen in the 3-D FSD measurements by Chen and Bilger [2]. The peak values of FSD for methane flames are systematically larger than those of propane flames. This is most probably due to the higher Lewis numbers of propane flames.

The mean direction cosine σ varied slightly through the whole range of u'/S_L between 0.64 to 0.72, and most values were around 0.65. This is very close to the typical value for Bunsen flames of 0.7 reported by Deschamps et al. [28] and the values of 0.55 to 0.65 reported by Chen and Bilger [2]. There is almost no change in the direction cosine across the flame front. All the direction cosine PDFs have shown very high peaks at $\sigma = 1.0$. Shepherd and Ashurst [34] have shown that 2-D and 3-D direction cosine PDFs are very similar and it is possible to estimate the true mean direction cosine from 2-D images. Current results have the same trend as shown by Shepherd and Ashurst [34]. The crossing angle has shown very little change

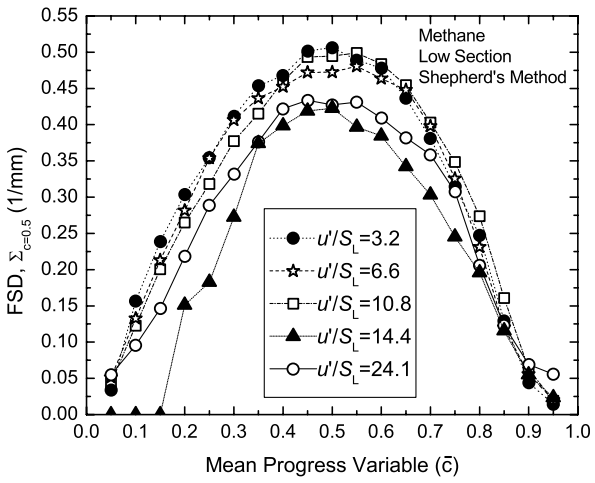

Fig. 17 FSD evaluated by Shepherd's method [25] at $c = 0.5$ as a function of mean progress variable (low section of methane flames).

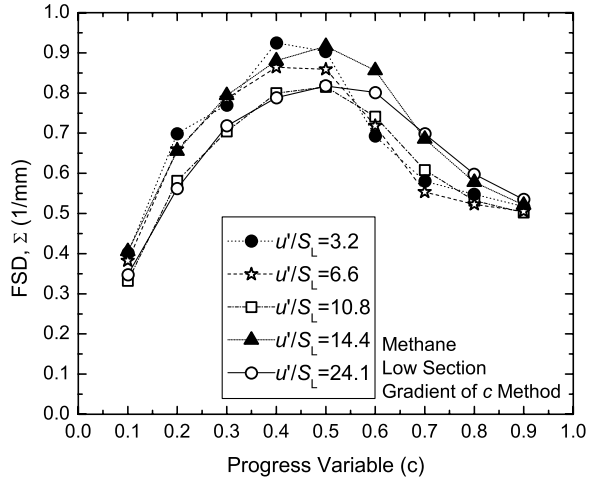

Fig. 18 FSD evaluated by the gradient of progress variable as a function of c (low section of methane flame).

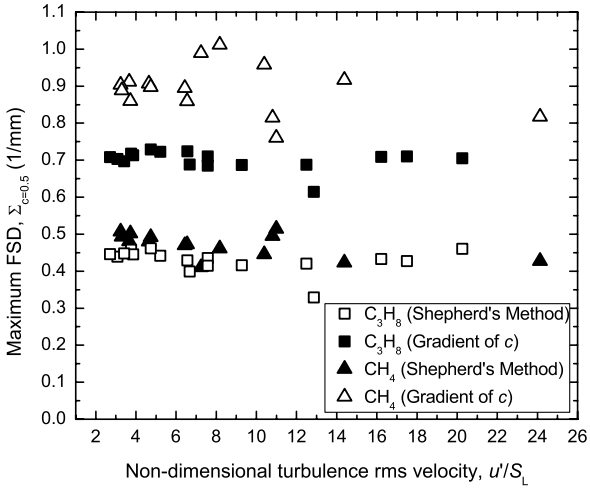

Fig. 19 Peak instantaneous FSD at $c = 0.5$ as a function of u'/S_L for methane and propane flames.

across the flame front and varies around 39–45 deg. The overall average is about 43.1 deg.

F. Variation of Flame Front Thickness and FSD with Curvature

To isolate the effects of curvature from other factors affecting the flame front structure, the variation of the reaction zone thickness, preheat zone thickness, and FSD results as a function of curvature were evaluated. This was done by making 80 uniform bins for the curvature statistics from -4 mm^{-1} to $+4$ mm^{-1}. Then the reaction zone thickness, preheat zone thickness, and FSD (evaluated by the gradient of c method) were averaged for each bin, which is similar to the method described by Robin et al. [35].

The variations of reaction zone thickness and preheat zone thickness with curvature are observed to have a v-shaped curve with the minimum around zero curvature $\kappa = 0$ and the thickness increased with increasing positive and negative curvature values. When curvature is zero, the flame front thickness is reduced by the combined effects of turbulent eddies and strain. However, flame stretch is primarily caused by curvature effects [32]. Thus, this thinning effect is largely attributed to the turbulent eddies. Soika et al. [4] have also shown the lowering of 3-D temperature gradient by positively curved flame elements. In the direct numerical simulation by Sankaran et al. [36], the results indicate that the flame becomes increasingly thicker with curvature and the lowest average flame thickness occurs at a slightly negative curvature, approximately equal to $1/\delta_L$. Similar trends were also observed for high pressure flames [37]. As shown in Fig. 20 for propane flames at $\phi = 0.7$, as u'/S_L increases, the reaction zone thickness decreases for $u'/S_L \leq 12.5$, which reinforces the idea of thinning of the flame front by turbulent eddies. The difference between reaction zone thickness changes for different u'/S_L values is higher for negative curvature than that of the positive curvature values. This implies that the amount of thinning is higher for negative curvatures when only the u'/S_L is changing. The same trend was also observed for methane flames at $\phi = 0.6$ as shown in Fig. 21.

The preheat zone thickness of propane flames at $\phi = 0.7$ increases as u'/S_L increases and an asymmetry was observed for higher u'/S_L (see Fig. 22), where positive curvature thickness values are higher than that of the negative curvature values. There is also a slight shift of the minimum thickness to the negative curvature side (at about -0.5 mm^{-1}). However, the methane preheat zone thickness slightly decreases as u'/S_L increases at higher positive curvature, as shown in Fig. 23. This is the opposite of the methane reaction zone thickness results, which implies that the modifications by curvature in the reaction zone and preheat zone might be different.

FSD data that are presented in the following were averaged instantaneous FSD values for each curvature bin value as described in the beginning of Sec. IV.F. The mean FSD value peaks at the zero curvature and it decreases with increasing and decreasing curvature, as seen in Fig. 24, for methane flames at $\phi = 0.6$. The mean FSD increases with increasing u'/S_L (Fig. 24). It could be argued that the turbulent eddies are thinning the flame front and thus increasing the amount of wrinkling of the flame, and the curvature effects are

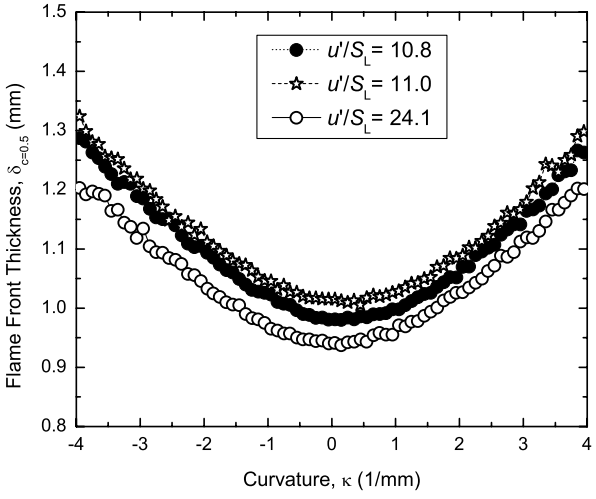

Fig. 21 Reaction zone thickness as a function of κ for methane flames at $\phi = 0.6$.

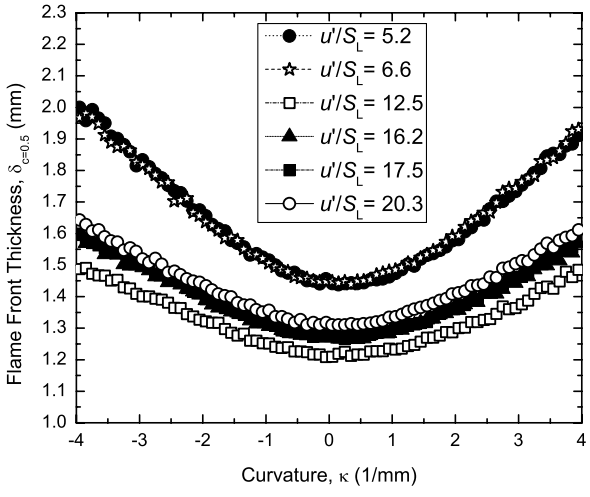

Fig. 20 Reaction zone thickness as a function of κ for propane flames at $\phi = 0.7$.

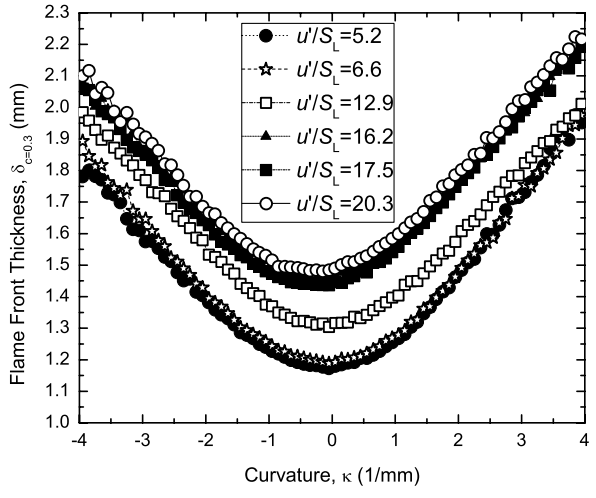

Fig. 22 Preheat zone thickness as a function of κ for propane flames at $\phi = 0.7$.

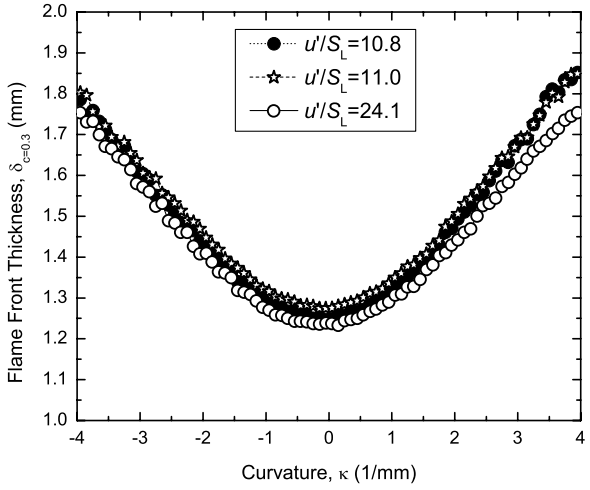

Fig. 23 Preheat zone thickness as a function of κ for methane flames at $\phi = 0.6$.

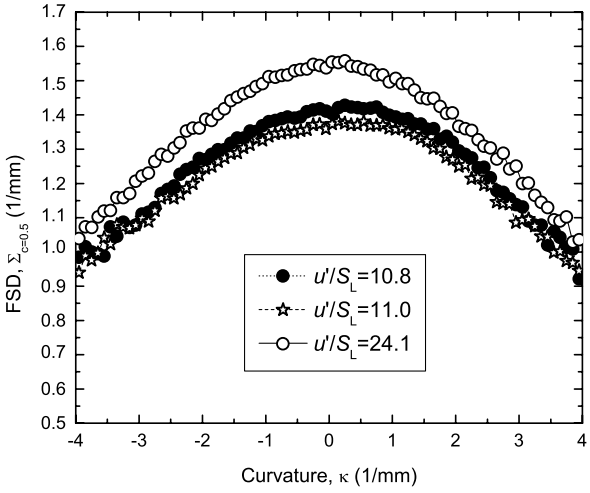

Fig. 24 Mean instantaneous FSD at $c = 0.5$, calculated using the gradient of c method, as a function of κ for methane flames at $\phi = 0.6$.

reducing the flame front wrinkling and flame surface area. Pope [38] suggests that turbulent straining tends to increase FSD, whereas the combined effects of curvature and flame propagation tends to decrease FSD. Because curvature and strain are both part of the stretch, which is mostly dominated by curvature [32], it might be argued that curvature and turbulent eddies are competing events during flame propagation. The changes in FSD for negative curvature between different u'/S_L are higher than that of the positive curvature. Negative curvature seems to able to increase reaction by increasing FSD and decrease reaction zone thickness. However, it seems that only curvature values around zero are capable to increase FSD. So curvature might work in conjunction with the turbulent eddies if the nondimensional turbulence intensity is high and the curvature values are close to zero. Although the curvature PDFs have the Gaussian distribution, which centered around zero, thickness results (reaction and preheat zone) still show an overall increase of thickness and a reduction of flame surface density.

Turbulent eddies are both creating the wrinkling (which is quantified here as the flame front curvature) and causing flame stretch. It may not be possible to completely isolate these two events; however, our conditional analysis of the curvature, flame thickness, and flame surface density imply that turbulent eddies decrease flame front thickness at locations where curvature is zero. On the other hand, the total effect of increasing turbulence intensity manifests itself as in increase in flame thickness.

V. Conclusions

The characteristics of turbulent premixed propane/air and methane/air flame front surfaces were examined using Rayleigh scattering in Bunsen-type methane and propane flames with u'/S_L from 2.7 to 24.1. Flame front thicknesses, temperature gradients, curvature statistics, and flame surface densities were measured. Modification of the averaged temperature profile was observed in the preheat zone of the flame front, accompanied by the slight broadening of reaction zone and preheat zone thicknesses with nondimensional turbulence intensity in both propane and methane flames. Flame front curvature statistics displayed a Gaussian distribution for all the flame conditions, and the mean curvature values decreased as a function of u'/S_L and approached zero. FSD estimated from both Shepherd's method and gradient of progress variable method for both fuels did not show any dependence on u'/S_L. Curvature was observed to affect the flame front by increasing its thickness and reducing FSD. Current results imply that the flame surface area might not be the dominant factor in increasing the turbulent burning velocity under the conditions corresponding to the thin reaction zones regime. This also suggests that the flamelet assumption may not be valid over the range of condition studied in this work, which means the validity range of the flamelet model may be more restricted than previously believed.

Acknowledgments

This research has been funded by a Natural Sciences and Engineering Research Council of Canada Collaborative Research Opportunity grant. The authors would like to thank N. Ashgriz for the loan of the particle image velocimetry system, and D. Pavé for his assistance in setting up the Rayleigh scattering system.

References

[1] Gülder, Ö. L., Smallwood, G. J., Wong, R., Snelling, D. R., Smith, R., Deschamps, B. M., and Sautet, J. C., "Flame Front Surface Characteristics in Turbulent Premixed Propane/Air Combustion," *Combustion and Flame*, Vol. 120, No. 4, 2000, pp. 407–416. doi:10.1016/S0010-2180(99)00099-1

[2] Chen, Y. C., and Bilger, R. W., "Experimental Investigation of Three-Dimensional Flame-Front Structure in Premixed Turbulent Combustion-I: Hydrocarbon/Air Bunsen Flames," *Combustion and Flame*, Vol. 131, No. 4, 2002, pp. 400–435. doi:10.1016/S0010-2180(02)00418-2

[3] Buschmann, A., Dinkelacker, F., Schäfer, T., Schäfer, M., and Wolfrum, J., "Measurement of the Instantaneous Detailed Flame Structure in Turbulent Premixed Combustion," *Proceedings of the Combustion Inst.*, Vol. 26, Pt. 1, 1996, pp. 437–445. doi:10.1016/S0082-0784(96)80246-3

[4] Soika, A., Dinkelacker, F., and Leipertz, A., "Measurement of the Resolved Flame Structure of Turbulent Premixed Flames with Constant Reynolds Number and Varied Stoichiometry," *Proceedings of the Combustion Inst.*, Vol. 27, Pt. 1, 1998, pp. 785–792. doi:10.1016/S0082-0784(98)80473-6

[5] Sinibaldi, J. O., Mueller, C. J., and Driscoll, J. F., "Local Flame Propagation Speeds Along Wrinkled, Unsteady, Stretched Premixed Flames," *Proceedings of the Combustion Inst.*, Vol. 27, Pt. 1, 1998, pp. 827–832. doi:10.1016/S0082-0784(98)80478-5

[6] Dinkelacker, F., Soika, A., Most, D., Hofmann, D., Leipertz, A., Polifke, W., and Döbbeling, K., "Structure of Locally Quenched Highly Turbulent Lean Premixed Flames," *Proceedings of the Combustion Inst.*, Vol. 27, Pt. 1, 1998, pp. 857–865. doi:10.1016/S0082-0784(98)80482-7

[7] Driscoll, J. F., "Turbulent Premixed Combustion: Flamelet Structure and its Effect on Turbulent Burning Velocity," *Progress in Energy and Combustion Science*, Vol. 34, No. 1, 2008, pp. 91–134. doi:10.1016/j.pecs.2007.04.002

[8] Peters, N., *Turbulent Combustion*, Cambridge Univ. Press, Cambridge, England, U.K.,2000, pp. 78–80.

[9] Dibble, R. W., and Hollenbach, R. E., "Laser Rayleigh Thermometry," *Proceedings of the Combustion Inst.*, Vol. 18, Pt. 1, 1981, pp. 1489–1499. doi:10.1016/S0082-0784(81)80151-8

[10] Eckbreth, A. C., *Laser Diagnostics for Combustion Temperature and*

Species, Gordon and Breach, New York, 2nd ed., 1996.
[11] Zhao, F. Q., and Hiroyasu, H., "The Application of Laser Rayleigh Scattering to Combustion Diagnostics," *Progress in Energy and Combustion Science*, Vol. 19, No. 6, 1993, pp. 447–485. doi:10.1016/0360-1285(93)90001-U
[12] Miles, R. B., Lempert, W. R., and Forkey, J. N., "Laser Rayleigh Scattering," *Measurement Science and Technology*, Vol. 12, No. 5, 2001, pp. R33–R51. doi:10.1088/0957-0233/12/5/201
[13] Knaus, D. A., Sattler, S. S., and Gouldin, F. C., "Three-Dimensional Temperature Gradients in Premixed Turbulent Glamelets via Cross-Plane Rayleigh Imaging," *Combustion and Flame*, Vol. 141, No. 3, 2005, pp. 253–270. doi:10.1016/j.combustflame.2005.01.008
[14] Sutton, J. A., and Driscoll, J. F., "Rayleigh Scattering Cross Sections of Combustion Species at 266, 355 and 532 N m for Thermometry Applications," *Optics Letters*, Vol. 29, No. 22, 2004, pp. 2620–2622. doi:10.1364/OL.29.002620
[15] Moffat, H. K., and Goodwin, D., "Cantera: Object-Orientated Software for Reacting Flow," http://www.cantera.org, June 2005.
[16] Galley, N., "Investigation of Thermal Flame Structure in Lean Turbulent Premixed Methane-Air Flames by Rayleigh Scattering," Master's Deg. Thesis, Univ. of Toronto, Inst. for Aerospace Studies, Toronto, June 2006.
[17] Kim, S. H., and Pitsch, H., "Scalar Gradient and Small-Scale Structure in Turbulent Premixed Combustion," *Physics of Fluids* Vol. 19, 2007, pp. 115104–115114. doi:10.1063/1.2784943
[18] Wang, G. H., and Clemens, N. T., "Effects of Imaging System Blur on Measurements of Flow Scalars and Scalar Gradients," *Experiments in Fluids*, Vol. 37, No. 2, 2004, pp. 194–205. doi:10.1007/s00348-004-0801-7
[19] Haq, M. Z., Sheppard, C. G. W., Woolley, R., Greenhalgh, D. A., and Lockett, R. D., "Wrinkling and Curvature of Laminar and Turbulent Premixed Flames," *Combustion and Flame*, Vol. 131, No. 1–2, 2002, pp. 1–15. doi:10.1016/S0010-2180(02)00383-8
[20] Chen, Y. C., "Measurement of Flame Front Curvature Based on Fourier Transformation," *Combustion Theory and Modelling*, Vol. 11, No. 3, 2007, pp. 333–349. doi:10.1080/13647830500348042
[21] Gülder, Ö. L., and Smallwood, G. J., "Flame Surface Densities in Premixed Combustion at Medium to High Turbulence Intensities," *Combustion Science and Technology*, Vol. 179, Nos. 1–2, 2007, pp. 191–206. doi:10.1080/00102200600808722
[22] Gülder, Ö. L., and Smallwood, G. J., "Do Turbulent Premixed Flame Fronts in Spark-Ignition Engines Behave Like Passive Surfaces?" *SAE Transactions: Journal of Engines*, Vol. 109, No. 3, 2001, pp. 1823–1832.
[23] Shepherd, I. G., and Cheng, R. K., "The Burning Rate of Premixed Flames in Moderate and Intense Turbulence," *Combustion and Flame*, Vol. 127, No. 3, 2001, pp. 2066–2075. doi:10.1016/S0010-2180(01)00309-1
[24] Gouldin, F. C., and Miles, P. C., "Chemical Closure and Burning Rates in Premixed Turbulent Flames," *Combustion and Flame*, Vol. 100, Nos. 1–2, 1995, pp. 202–210. doi:10.1016/0010-2180(94)00121-8
[25] Shepherd, I. G., "Flame Surface Density and Burning Rate in Premixed Turbulent Flames," *Proceedings of the Combustion Inst.*, Vol. 26, Pt. 1, 1996, pp. 373–379. doi:10.1016/S0082-0784(96)80238-4
[26] Pope, S. B., "The Evolution of Surfaces in Turbulence," *International Journal of Engineering Science*, Vol. 26, No. 5, 1988, pp. 445–469. doi:10.1016/0020-7225(88)90004-3
[27] Shepherd, I. G., Cheng, R. K., Plessing, T., Kortschik, C., and Peters, N., "Premixed Flame Front Structure in Intense Turbulence," *Proceedings of the Combustion Inst.*, Vol. 29, Pt. 2, 2002, pp. 1833–1840. doi:10.1016/S1540-7489(02)80222-X
[28] Deschamps, B. M., Smallwood, G. J., Prieur, J., Snelling, D. R., and Gülder, Ö. L., "Surface Density Measurements of Turbulent Premixed Flames in a Spark-Ignition Engine and a Bunsen-type Burner Using Planar Laser-Induced Fluorescence," *Proceedings of the Combustion Inst.*, Vol. 26, Pt. 1, 1996, pp. 427–435. doi:10.1016/S0082-0784(96)80245-1
[29] Smallwood, G. J., and Deschamps, B. M., "Flame Surface Density Measurements with PLIF in an SI Engine," SAE Technical Paper Series, No. 962088, 1996, pp. 427–435.
[30] Kortschik, C., Plessing, T., and Peters, N., "Laser Optical Investigation of Turbulent Transport of Temperature Ahead of the Preheat Zone in a Premixed Flame," *Combustion and Flame*, Vol. 136, Nos. 1–2, 2004, pp. 43–50. doi:10.1016/j.combustflame.2003.09.018
[31] de Goey, L. P. H., Plessing, T., Hermanns, R. T. E., and Peters, N., "Analysis of the Flame Thickness of Turbulent Flamelets in the Thin-Reaction Zone Regime," *Proceedings of the Combustion Institute*, Vol. 30, Pt. 1, 2005, pp. 859–866. doi:10.1016/j.proci.2004.08.016
[32] Law, C. K., "Dynamics of Stretched Flames," *Proceedings of the Combustion Inst.*, Vol. 22, Pt. 1, 1988, pp. 1381–1402 doi:10.1016/S0082-0784(89)80149-3.
[33] Chen, Y. C., Kim, M., Han, J., Yun, S., and Yoon, Y., "Analysis of Flame Surface Normal and Curvature Measured in Turbulent Premixed Stagnation-Point Flames with Crossed-Plane Tomography," *Proceedings of the Combustion Inst.*, Vol. 31, Pt. 1, 2007, pp. 1327–1335. doi:10.1016/j.proci.2006.08.023
[34] Shepherd, I. G., and Ashurst, W. M. T., "Flame Front Geometry in Premixed Turbulent Flames," *Proceedings of the Combustion Inst.*, Vol. 24, Pt. 1, 1992, pp. 485–491. doi:10.1016/S0082-0784(06)80062-7
[35] Robin, V., Mura, A., Champion, M., Degardin, O., Renou, B., and Boukhalfa, M., "Experimental and Numerical Analysis of Stratified Turbulent *V*-shaped Flames," *Combustion and Flame*, Vol. 153, Nos. 1–2, 2008, pp. 288–315. doi:10.1016/j.combustflame.2007.10.008
[36] Sankaran, R., Hawkes, E. R., Chen, J. H., Lu, T. F., and Law, C. K., "Structure of a Spatially Developing Turbulent Lean MethaneAir Bunsen Flame," *Proceedings of the Combustion Inst.*, Vol. 31, Pt. 1, 2007, pp. 1291–1298. doi:10.1016/j.proci.2006.08.025
[37] Halter, F., Chauveau, C., and Gökalp, I., "Investigation on the Flamelet Inner Structure of Turbulent Premixed Flames," *Combustion Science and Technology*, Vol. 180, No. 4, 2008, pp. 713–728. doi:10.1080/00102200701851266
[38] Pope, S. B., "Computations of Turbulent Combustion: Progress and Challenges," *Proceedings of the Combustion Inst.*, Vol. 23, Pt. 1, 1990, pp. 591–612. doi:10.1016/S0082-0784(06)80307-3

R. Lucht
Associate Editor